

Autonomous Underwater Vehicle-Based Concurrent Detection and Classification of Buried Targets Using Higher Order Spectral Analysis

Monica Montanari, Joseph R. Edwards, and Henrik Schmidt

Abstract—This paper presents a processing concept for autonomous underwater vehicle (AUV)-based concurrent detection and classification (CDAC) of mine-like objects. In the detection phase, the AUV seeks objects of interest using a simple energy detector combined with a peak tracking mechanism. Upon detection, the processing mechanism changes to a higher order spectral (HOS) classification process. The system is demonstrated through theory, simulation and at-sea experiments to have promise in reducing the false alarm rate of mine detections. The HOS classification mechanism is also shown to have some benefit over classical spectral estimation in all cases. Components of the system concept were also demonstrated live onboard the AUV during the Generic Oceanographic Array Technology Sonar (GOATS 2002) experiment off the coast of Italy, while others are demonstrated using a comprehensive AUV sonar simulation framework.

Index Terms—Autonomous underwater vehicle, concurrent target detection and classification, higher order spectral analysis, spectral analysis.

I. INTRODUCTION

RECENT rapid developments in autonomous underwater vehicle (AUV) technology have provided the opportunity to explore new approaches for detecting and classifying mine-like objects. Since its inception in 1998, the Office of Naval Research (ONR)/NATO SACLANT Undersea Research Center/Massachusetts Institute of Technology (MIT) Generic Oceanographic Array Technology Sonar (GOATS) joint research project has been simultaneously focused on developing the AUV technology and these new mine classification approaches. Of particular interest in this project has been the use of different vehicle processing or behavioral modalities within the course of a single mission in order to achieve concurrent detection and classification (CDAC) of mine-like objects, which represents a step in the direction of truly autonomous AUVs from the current state of the art of preprogrammed surveying and postprocessing of the received data and images [1], [2]. Varying the behavioral modality would include utilizing the mobility of the vehicles to facilitate deformable sonar geometries that can be adaptively controlled based on the

local acoustic scattering statistics. Preferred target scattering directions for both specular and, more importantly, elastic scattering returns can be interrogated by the adaptively controlled receiver platforms [3]. The topic of behavioral adaptation is briefly covered in Section IV-C, but is not the focus of this paper. More directly addressed in this paper is the variance of processing modalities, in which the onboard signal processing of the vehicle changes from detection phase to classification phase. With this method, the CDAC process is concurrent in the sense that the detection and the classification occur without user intervention during the course of a single mission, but is still divided into two steps: detection, then classification. The detection step is discussed in Section II, and the classification step in Section III. The balance of the paper is dedicated to illustrative examples of the application of these adaptive algorithms, ranging from full acoustic simulations to real-time at-sea AUV implementations.

II. ADAPTIVE TARGET DETECTION

In the first stage of a mine hunting mission, the AUV flies on a preplanned path while using its active sonar. The received echoes are continuously analyzed by the processing system onboard the AUV and useful information is extracted and stored, such as the statistics of the local reverberation and useful environmental parameters. In general, the extracted information as well as the signal data may be transmitted to the base station. A more advanced and challenging configuration would be to employ multiple AUVs, with a single source and multiple receivers [1]. In this case each vehicle communicates with the others, as well as with the offshore base station. However, to be consistent with the actual at-sea experiments, only a single monostatic AUV is considered here.

During the searching stage the bulk of the processing is devoted to target detection. The adaptive target detector developed in this paper is supported by a tracking algorithm in order to detect and discriminate targets of interest against strong reverberation echoes from clutter and interfering noise sources. A detection is declared when the preprocessed received signal is higher than the threshold, which is adaptively computed and depends on the local environment. Consider the vehicle outfitted with a linear sonar receiver array configuration consisting of L elements, and carrying a source that transmits P pings on the insonified region. For a specific element or (for beam-time preprocessed data) angle, each ping is sampled at the sampling fre-

Manuscript received September 15, 2003; revised September 11, 2005; accepted December 30, 2005. This work was supported by Office of Naval Research (ONR). Associate Editors: A. Baggeroer and J. F. Lynch.

M. Montanari is with VASA Associates, McLean, VA 22102 USA (e-mail: monica.montanari@gmail.com).

J. R. Edwards and H. Schmidt are with the Center for Ocean Engineering, Massachusetts Institute of Technology, Cambridge, MA 02139 USA.

Digital Object Identifier 10.1109/JOE.2006.872216

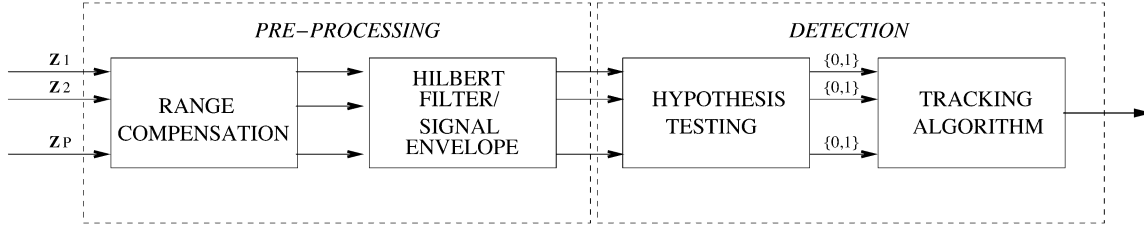


Fig. 1. Block diagram of the target detection algorithm.

quency f_s and the number of samples per ping is N . Denote with

$$\mathbf{z}_p = [z_p(0) z_p(1) \cdots z_p(N-1)]^T \quad (1)$$

the $(N \times 1)$ -dimensional vector relative to a generic sensor and comprising the received N signal samples for ping p , with $p = 1, 2, \dots, P$. In the following, H_0 represents the null hypothesis, which corresponds to only reverberation in the received signal and H_1 represents the alternative hypothesis, which corresponds to a target in the insonified field. The detection problem is stated as a binary hypothesis test

$$\begin{cases} H_0 : \mathbf{z}_p = \mathbf{r}_p \\ H_1 : \mathbf{z}_p = \mathbf{s}_p + \mathbf{r}_p \end{cases} \quad (2)$$

where \mathbf{r}_p and \mathbf{s}_p are respectively the reverberation and the target signal vectors relative to the p th ping. The overall target detection algorithm is depicted schematically in Fig. 1, where the pre-processor and the actual detector are highlighted. The pre-processor block computes the envelope of the range-compensated signal $\tilde{\mathbf{z}}_p = |\mathbf{z}_p + j\mathcal{H}(\mathbf{z}_p)|$, where $\mathcal{H}(\cdot)$ denotes the Hilbert transform operator. The envelope is written here in terms of the Hilbert transform because the broadband signal is analytic [4] and sufficiently wideband that demodulation is not useful and therefore not done. This expression of the envelope is also consistent with the onboard processing implementation used at sea. The block following the preprocessor in Fig. 1 performs the actual detection task, comparing the envelope $\tilde{\mathbf{z}}_p$ of the received signal to a threshold T_p and declaring a candidate target presence each time a peak in the envelope is higher than the threshold. The threshold T_p is computed adaptively from the data as

$$T_p = E\{\tilde{\mathbf{z}}_p\} + \gamma \sqrt{E\{(\tilde{\mathbf{z}}_p - E\{\tilde{\mathbf{z}}_p\})^2\}} \quad (3)$$

where $E\{\cdot\}$ denotes the statistical expectation operator and γ is a positive real coefficient which determines the admissible deviation from the mean value and fixes the false alarm rate for single-ping operations. The choice of the threshold setting as defined in (3) is suitable in applications like this, where the target return is a peak over a background of reverberation and is particularly appealing due to the simplicity of the calculation and to the fact that it does not require any *a priori* knowledge of the target and reverberation signal models.

In practice, there is no direct access to the ensemble quantities, so the sample expectation is employed

$$T_p = \frac{1}{N} \sum_{n=0}^{N-1} \tilde{z}_p(n) + \gamma \sqrt{\frac{1}{N} \sum_{n=0}^{N-1} \left(\tilde{z}_p(n) - \frac{1}{N} \sum_{n=0}^{N-1} \tilde{z}_p(n) \right)^2} \quad (4)$$

After the threshold level has been set, each peak in the backscattered signal is compared to the threshold level, performing the binary hypothesis test

$$\tilde{z}_p(n_i) \underset{H_0}{\overset{H_1}{\geq}} T_p \quad (5)$$

where n_i denotes the vector index corresponding to the i th peak in $\tilde{\mathbf{z}}_p$. The case $i > 1$ corresponds to multiple candidate targets in the insonified patch. If the received signal is higher than the threshold, but there is no real target in the insonified patch, a false alarm occurs.

A peak tracking strategy that processes multiple adjacent pings is necessary to improve the rejection of false targets, such as clutter and interfering sources. To this purpose, the single-ping detection algorithm of (5) is run over each ping and the detections at each ping are tracked over several pings using basic physical principles in order to establish which of the single-ping detections qualifies as a target of interest. The peak tracking is performed inside a fixed-length window centered on the previous ping arrival time. The arrival time shifting is due to the AUV-target distance, which varies as the AUV moves. The length of the window is set to be a fraction of the maximum time shift measured between two successive pings. This maximum shift occurs when the target is aligned with the AUV path and is calculated as

$$\Delta_{t_{\max}} = |t_i - t_{i+1}| = \frac{2R_{i,i+1}}{c} = \frac{2v \cdot pr}{c} \quad (6)$$

where t_i denotes the target arrival time for ping i , $R_{i,i+1}$ is the distance traveled during the ping rate pr , v is the AUV speed, and c is the sound speed. Once a target detection has been declared at time t_i , the next target arrival time t_{i+1} is expected to lie inside the window centered on t_i . A target tracking is performed as long as the arrival time lies inside the window whose center position is updated at each ping. If we set the window length to be a tenth of the maximum time shift $\Delta_{t_{\max}}$, the window length measured in samples can be written as

$$\Delta_s = \frac{\Delta_{t_{\max}} f_s}{10} = \frac{v \cdot pr \cdot f_s}{5c}. \quad (7)$$

The overall trajectory of the detections is further restricted to follow an incoming-outgoing path consistent with a compact

target, expressed simply as a hyperbolic variation in range. The motivation for this restriction is so the AUV will reject direct bounces from the seafloor, which is clearly a noncompact target. The hyperbolic model arises from the fact that an AUV flying along a straight line past a compact target creates a trajectory in the ping number-sample number plane that is a branch of a hyperbola. An application of the proposed detection algorithm to experimental data is discussed in Section IV-B

III. TARGET CLASSIFICATION

The classification of detected targets into mine-like objects or rock-like objects has a crucial importance in a mine hunting mission because of the potential of finding many rocks for each mine-like target of interest. Reducing this false alarm rate allows the mine-hunting system to operate much more efficiently and cover more area in less time. For this reason, automated target classification methods have been studied at length in recent years. In both sonar and radar, the typical approach to target recognition is to train the processor with modeled or archived data and extract features. The fundamental differences within this approach to classification primarily lies within the feature extractor and the means by which the correlated clutter is reduced. An example of recent model-based target classification uses a correlation technique across multiple aspects, applying the argument that the clutter decorrelates across angles while some of the target features do not [5]. Other recent sonar studies have classified targets in this manner through hidden Markov models [6] over multiple target aspects, inherently applying the same clutter reduction premise. Recent work in radar applies a more direct approach by adaptively filtering the clutter prior to the template-based recognition correlation [7]. The classification procedure proposed in this paper, on the other hand, employs nonparametric methods to enhance the detection of an elastic response in the signal backscattered from the object. The nonparametric approach is used due to an assumed lack of *a priori* knowledge regarding both the clutter content and the object type, burial condition and aspect during the course of an extended AUV mission. Further, the classification is made only on the part of the return immediately following the specular return, because these postspecular oscillations reveal characteristics of the target while the specular return is less sensitive to target type. It has also been shown that for buried targets, the low-pass filtering effect of the seabed has a strong influence on the specular return [8]. Rocks and boulders do not exhibit coherent structural waves, which on the contrary are a characteristic of man-made objects, such as mines at more regular geometry. The elastic waves are strongly aspect- and object-dependent and are delayed in time with respect to the specular return due to the fact that the waves must travel around the object in order to build the target resonance. To capture this delayed return, a temporal window is set after the specular return of each detected target for the investigation of the elastic response presence. The length of the window is related to the characteristic dimension of the target and must be chosen as a compromise between two opposite needs: it should be long enough to contain the main elastic component and short enough to avoid interfering signals from nearby targets. This procedure performs

the classification task as a binary hypothesis test for each target: The weak elastic response must be detected inside the search window, in the presence of correlated reverberation. To this purpose, higher order spectral (HOS) analysis techniques are employed in this paper, in particular the second and third-order cumulant spectra are considered, and their definitions are given hereafter.

For a zero mean stationary process, the second-order cumulant $c_2^z(\tau)$ and the third-order cumulant $c_3^z(\tau_1, \tau_2)$ are identical to the second and third-order moments, respectively $m_2^z(\tau)$ and $m_3^z(\tau_1, \tau_2)$ [9], which are defined as

$$m_2^z(\tau) \triangleq E\{z(n) \cdot z(n + \tau)\} \quad (8)$$

$$m_3^z(\tau_1, \tau_2) \triangleq E\{z(n) \cdot z(n + \tau_1) \cdot z(n + \tau_2)\} \quad (9)$$

where τ, τ_1 , and τ_2 denote the time differences. The second-order moment spectrum is the power spectral density (PSD) of the signal, and is calculated as the Fourier transform of the second-order moment, or covariance sequence. The third-order spectrum has a particular advantage in rejecting Gaussian noise, since the third moment of a zero mean Gaussian process is identically zero. Although the reverberation is not expected to be Gaussian, the random scattering from the seabed, combined with the wide insonification angle of the source, creates a situation in which the local (in time) signal is nearly Gaussian. An intuitive explanation of this phenomenon is that the wide source angle causes the reflection from a large number of independent scatterers to arrive at nearly the same time, creating a quasi-Gaussian distribution due to the central limit theorem. A more detailed formulation has been given by Doisy [10]. This temporal Gaussianity is shown empirically in Fig. 2. In this plot, the distribution of the time signals received by an AUV-borne monostatic sonar during a mission is shown for several given ranges, and compared to the expected Gaussian distribution. The more narrow distributions correspond to shorter ranges, and the distributions flatten out with range, as a result of the increased number of independent scatterers. As expected, the distributions agree well with the Gaussian assumption.

The second-order cumulant spectrum can be written as

$$C_2^z(\omega) = M_2^z(\omega) = \sum_{\tau=-\infty}^{+\infty} m_2^z(\tau) e^{-j\omega\tau} \quad (10)$$

where $|\omega| \leq \pi$. The third-order cumulant spectrum is named bispectrum and for a zero mean stationary signal is calculated as

$$\begin{aligned} C_3^z(\omega_1, \omega_2) &= M_3^z(\omega_1, \omega_2) \\ &= \sum_{\tau_1=-\infty}^{+\infty} \sum_{\tau_2=-\infty}^{+\infty} m_3^z(\tau_1, \tau_2) e^{-j(\omega_1\tau_1 + \omega_2\tau_2)} \end{aligned} \quad (11)$$

where $|\omega_1|, |\omega_2| \leq \pi$ and $|\omega_1 + \omega_2| \leq \pi$. Due to the symmetry conditions deriving from the properties of the moments, it is sufficient to know the bispectrum in the triangular region $\omega_2 \geq 0, \omega_1 \geq \omega_2, \omega_1 + \omega_2 \leq \pi$ to completely describe the bispectrum [9]. Moreover, the frequency domain is divided into 12 symmetry regions for real processes, so the calculation of the

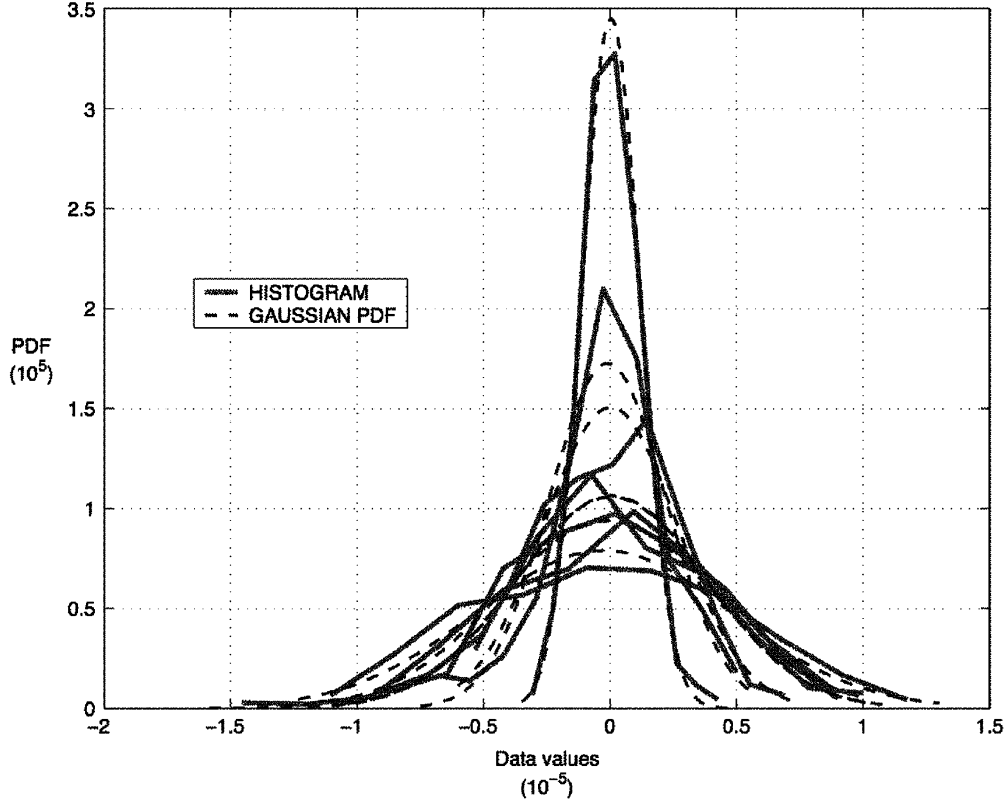


Fig. 2. Histograms of the reverberation data from the GOATS experiment, compared to the Gaussian distribution.

bispectrum can be performed very efficiently by employing fast Fourier transform (FFT) techniques.

The PSD $C_2^z(\omega)$ is estimated by using the Blackman–Tukey technique [11]

$$\hat{C}_2^z(\omega) = \sum_{\tau=-M+1}^{M-1} \hat{m}_2^z(\tau) w(\tau) e^{-j\omega\tau} \quad (12)$$

where $w(\tau)$ is a filtering window, with length $M < N$, $\hat{m}_2^z(\tau) = 1/N \sum_{n=\tau+1}^{N-1} z(n)z(n-\tau)$ and $\hat{m}_2^z(-\tau) = \hat{m}_2^z(\tau)$, for $0 \leq \tau \leq N-1$, is the estimated second-order moment of the process $z(n)$. The filtering window is an even function, which decays smoothly to zero and is such that $w(0) = 1$ and $w(\tau) = 0$ for $|\tau| \geq M$. The choice of a non parametric method, such as the Blackman–Tukey procedure, is motivated by the fact that there is no *a priori* knowledge of the spectrum model. Moreover, the Blackman–Tukey method is preferred over the periodogram, because the latter is biased and has a variance which does not decrease with the number of samples. On the contrary, the Blackman–Tukey estimator, acting like a locally weighted average of the periodogram, reduces the high statistical variations [11].

The bispectrum $C_3^z(\omega_1, \omega_2)$ is estimated as

$$\begin{aligned} \hat{C}_3^z(\omega_1, \omega_2) &= \sum_{\tau_1=-L_3}^{L_3} \sum_{\tau_2=-L_3}^{L_3} \left\{ \hat{m}_3^z(\tau_1, \tau_2) \cdot w(\tau_1, \tau_2) e^{-j(\omega_1\tau_1 + \omega_2\tau_2)} \right\} \\ & \quad (13) \end{aligned}$$

where $\hat{m}_3^z(\tau_1, \tau_2)$ is the second-order moment estimated with the indirect method described in [9], L_3 the region of support of $\hat{m}_3^z(\tau_1, \tau_2)$, and $w(\tau_1, \tau_2)$ is the filtering window.

After the calculation of the PSD or bispectrum of the total signal and the corresponding reverberation-only signal, a simple classification algorithm computes the gain of the signal with respect to the reverberation and decides for the presence or absence of the elastic response following the specular response. A gain corresponds to a man-made target classification; on the contrary, a unit gain corresponds to a natural object classification. The classification parameters are defined as follows. For the second-order statistic the gain γ_2 is defined as

$$\gamma_2 = \frac{\int_{\omega} \frac{C_2^z(\omega)}{C_2^r(\omega)} d\omega}{\int_{\omega} \frac{C_2^z(\omega)}{C_2^r(\omega)} d\omega} = \frac{\int_{\omega} \frac{C_2^z(\omega)}{C_2^r(\omega)} d\omega}{B} \quad (14)$$

where $C_2^r(\omega)$ is the reverberation PSD and B is the bandwidth. The classification parameter computed from the third-order statistics is named γ_3 and is defined as

$$\begin{aligned} \gamma_3 &= \frac{\int_{\omega_1} \int_{\omega_2} \frac{|C_3^z(\omega_1, \omega_2)|}{|C_3^r(\omega_1, \omega_2)|} d\omega_1 d\omega_2}{\int_{\omega_1} \int_{\omega_2} \frac{|C_3^z(\omega_1, \omega_2)|}{|C_3^r(\omega_1, \omega_2)|} d\omega_1 d\omega_2} \\ &= \frac{\int_{\omega_1} \int_{\omega_2} \frac{|C_3^z(\omega_1, \omega_2)|}{|C_3^r(\omega_1, \omega_2)|} d\omega_1 d\omega_2}{B_1 B_2} \quad (15) \end{aligned}$$

TABLE I
WATER COLUMN AND BOTTOM PARAMETER VALUES

Parameter	Value
c_1	1500 m/s
ρ_1	1000 kg/m ³
c_2	1700 m/s
ρ_2	1800 kg/m ³
l_0	1 m
σ_c	0.01
θ_{gr}	30°

where again $C_3^r(\omega_1, \omega_2)$ is the reverberation bispectrum and B_1 and B_2 are the bandwidths relative to the bidimensional frequency domain. Both performance measures are normalized so that they can be compared with one another.

The results from the PSD and bispectrum estimation using real data collected during the GOATS 1998 and the GOATS 2002 experiments, as well as simulated data, are discussed in Section IV-D. The discrimination of the elastic response from the reverberation requires the estimation of the reverberation spectra. Thus, the spectra of the total signals are compared to the spectra of the reverberation-only signals, relative to the same investigation area. This information is available to the AUV during the first stage of the mine hunting mission, prior to when any target detection has occurred. The numerical analysis demonstrates that the bispectrum improves the gain γ with respect to the PSD, thus leading to improved classification performance in low signal-to-noise ratio (SNR) scenarios.

IV. EXAMPLES

A. Analysis Tools

1) *The Goats 1998 Experiment:* The GOATS 1998 experiment took place in Marciana Marina, off the coast of Isola d'Elba, Italy. The GOATS 1998 experimental data used in this example were collected by an AUV flying between a fixed source, positioned in a tower, and the target field containing a two fully buried spheres and a half buried sphere. The pings processed in this example are collected when the AUV drives close to the source, so the configuration may be considered as monostatic. The water column and sea bottom parameter values are reported in Table I and represent a fair reproduction of both GOATS experimental environments. In Table I c_1 and ρ_1 are the sound speed and the density in water, respectively; c_2 and ρ_2 represent the same quantities in the bottom sediment; l_0 is the bottom horizontal correlation length; σ_c is the standard deviation of the sound speed in the inhomogeneous region, relative to the sound speed c_2 ; θ_{gr} is the grazing angle. The source central frequency is $f_c = 8$ kHz; the bandwidth is about 9 kHz; the sampling frequency is $f_s = 50$ kHz. The length of the elastic window for a 1 m diameter sphere is chosen to be 2 ms for the considerations discussed in Section III.

2) *The Goats 2002 Experiment:* The GOATS 2002 experiment was held in the Ligurian Sea off the coast of Italy in June 2002. This experiment employed one Bluefin Odyssey III class AUV, named *Caribou*, which was outfitted with two parallel

eight element linear arrays in a swordfish style. The data processed in this example were collected in a mission where the source had a central frequency $f_c = 15$ kHz and a bandwidth of 20 kHz, the sampling frequency was $f_s = 100$ kHz, and the nominal half-beamwidth of the source was 20°. The vehicle moved at approximately 1.5 m/s over a preplanned "sliding box" trajectory over a target field containing approximately 15 cement blocks that permanently exist in this area. The water depth in the target region varied from 20–30 m and the vehicle attempted to maintain a constant depth of 5 m. The simple detection algorithm described in Section II ran continuously during this 20 min mission. The ping rate was $pr = 1s^{-1}$ and the window length for the tracking algorithm was $\Delta_s = 20$ samples.

3) *The SEALAB Acoustic Simulation Tool:* The SEALAB simulation tool relies on wave scattering theory and was developed by VASA Associates. The acoustic simulator generates time series for arbitrary source/receiver geometries, including direct path, multipaths, roughness scattering, and target scattering components. The targets included are exact theoretical solutions of fluid-filled spherical and cylindrical elastic shells [12]. Although the target scattering theory is well developed, the boundary conditions along the outside of the buried target are very difficult to accurately model. The boundary conditions influence the amplitudes and frequencies of resonance of the targets, so the elastic behavior of the simulated targets may not precisely match the real target behavior. The simulation tool generates the reverberation process by calculating the scattering from a random realization of the rough bottom interface. In real situations, the bottom backscattered signal is generated by two different processes: volume and surface scattering. The volume scattering dominates the lower frequencies, while the surface scattering dominates the higher frequencies. Of course, for buried targets, as those of interest here, volume scattering assumes a strong role. However, the simulation includes only surface roughness scattering.

B. Detection Example

This section shows a real-time onboard detection example that was achieved during the GOATS 2002 experiment. The actual implementation onboard the vehicle is indicated by the block scheme depicted in Fig. 3. The nose array of the vehicle collects acoustic data after each ping, which is discretized by the DSP card to 10 000 samples per element per ping. The DSP card then saves the digital data to disk, managed by the mission-oriented operating system (MOOS) of the AUV [13]. The detection algorithm runs continuously as a client of the operating system, and begins to analyze the new data each time the MOOS informs it of the location and name of the new data files. The detection algorithm retains the locations of possible targets, i.e., those that have met the thresholding criterion in (5), and returns detection declarations to the MOOS when one of these possible targets is tracked over ten consecutive pings.

The onboard implementation of the tracking algorithm was simplified greatly due to the computational resources available on the AUV, which included a Pentium I processor-based CPU. The limited computational resources allowed only broadside beamforming, reducing the receiver array to essentially a

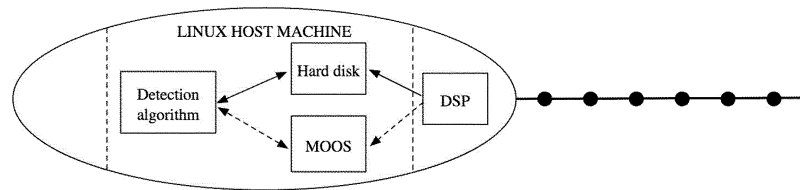


Fig. 3. Processing blocks for detection on board the AUV in the GOATS 2002 experiment.

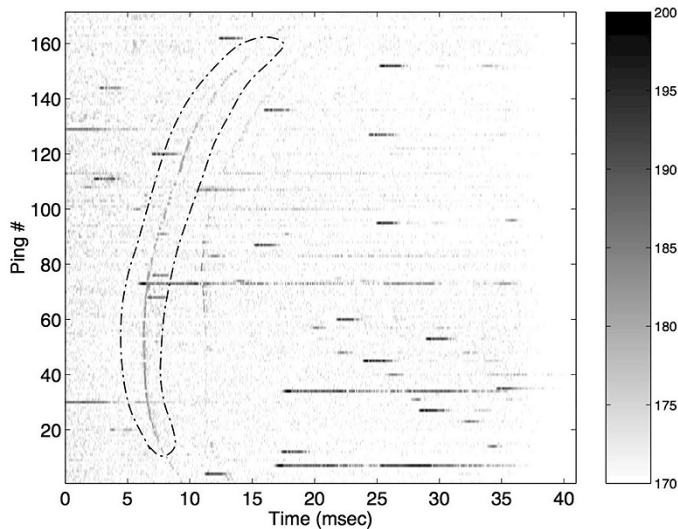


Fig. 4. Online detections performed on board the AUV in the GOATS 2002 experiment.

range-only sensor. The tracking algorithm then allowed the local detections to follow only a hyperbolic-type trajectory, allowing some sway in the vehicle motion, to be classified as a target of interest. Over the course of the mission in this example, the detection algorithm detected and reported 16 targets of interest to the MOOS. One such target detection is shown in Fig. 4, where the amplitude of the received echoes is reported as a function of ping and sample number. The target of interest lies 60 m in slant range from the closest point of approach of the AUV. The detected target is highlighted inside the dashed window, while other interfering noise sources, such as the intermittent echo sounder of the R/V Alliance that is seen throughout the plot and the onboard acoustic modem seen as extended noise sources (horizontal lines), are discarded by the tracking algorithm. Upon detection, the AUV simply reported the ping number and estimated location of the target to the MOOS, which in turn recorded this information in the vehicle log. Because MOOS also controls the navigation and propulsion hardware, it was envisioned that the vehicle would take some appropriate action at this point to further investigate the target of interest. Unfortunately, mechanical and time issues prevented the vehicle to assume adaptive independent behavior during the experiment, but an example of such adaptive behavior using simulated data is discussed in the following subsection. This example and other results from both experimental and simulated data, which are not reported here for brevity, demonstrate that this detection algorithm provides a capability to rapidly detect targets while discarding false alarms from various interferers, including both nonstationary and

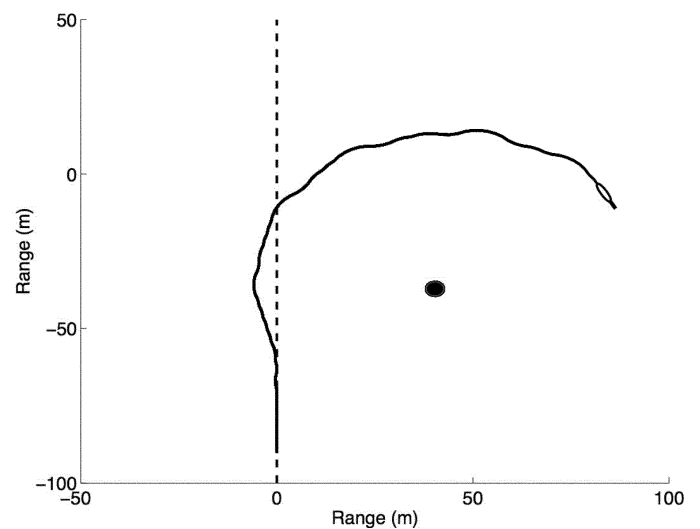


Fig. 5. Simulated mission with adaptive AUV path planning.

noncompact targets. These attributes allow a minimal number of targets, limited to those that are stationary and compact, to be passed into the classification stage.

C. Adaptive AUV Path Planning

Sensor-adaptive AUV missions are commonly implemented for reasons of vehicle safety, e.g., mission abort commands for exceeding depth or time constraints. On the other hand, sonar-based adaptivity to meet mission objectives represents a significant increase in AUV capabilities and has not yet been widely pursued. Attempts at sonar-adaptive behaviors have not yet been implemented extensively, due to hardware constraints and limited mission availability, but are expected to become increasingly prominent in future operations. In the context of this paper, sonar-adaptive AUV behavior would occur between the detection stage and the classification stage. This adaptivity seeks to mimic the behavior of the current kings of mine classification, bottlenose dolphins [14], [15]. Upon detecting a target during the course of its mission, the AUV, like the dolphin, would swim to a series of perspectives that are advantageous for classifying the target. This capability has been demonstrated with full SEALAB acoustic simulations and real-time simulations on the vehicle operating system using experimental data in replay mode, but has not yet been achieved onboard the AUV during a mission. An example simulated mission is shown in Fig. 5. In this simulation, a 1 m diameter proud rigid sphere is located at the origin. The frequency is 8 kHz and the vehicle has an 8-element nose array with a uniform spacing of 0.1 m. The seabed has a sound speed of 1800 m/s and a shear speed of 600 m/s. The

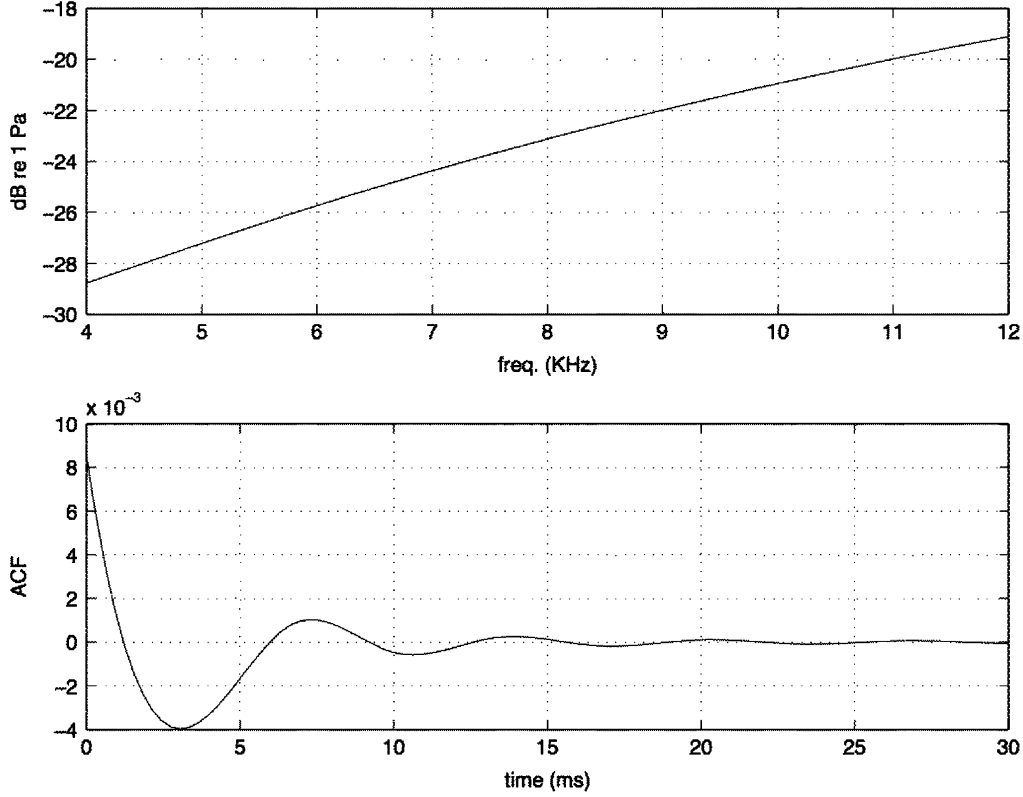


Fig. 6. Theoretical reverberation power spectral density (PSD) and autocorrelation function (ACF) from an incident plane wave.

AUV pings three times per second. All of the relevant parameters were chosen to closely match the actual conditions of the GOATS experiments. The AUV is assigned a preprogrammed trajectory that passes near the target, given by a straight-line path from the lower left of the figure at a heading of 75° , and represented by the dashed line in the figure. The actual path of the AUV is shown as a solid line. At the beginning of the mission, the AUV attempts to follow the preprogrammed trajectory at a speed of 1.5 m/s. The deviation from the preprogrammed path in this stage of the mission is attributable to a Gaussian-distributed heading uncertainty with a standard deviation of 3° that is included to approximate the actual compass sensor performance. The scattered signals from the seabed and target are received by the vehicle and searched for targets. The target detection statistic is given by the following:

$$\Gamma_p(x, y) = \frac{R_p^2 R_{p+1}^2}{\text{std} \{ |b_p(R_p, 0^\circ)| \} \text{std} \{ |b_{p+1}(R_{p+1}, 0^\circ)| \}} \quad (16)$$

where R_p is the range from the vehicle position at ping p to the pixel (x, y) , $b_p(R_p, 0^\circ)$ is the beamformer output at broadside at the appropriate range, and std is the standard deviation operator. Broadside beamforming was employed in the simulation to match the conditions on the vehicle, as discussed in Section IV-B. If a target is detected at the same point for 20 consecutive pings using the adaptive procedure described in Section II, then it is declared a target of interest and the AUV is allowed

to pursue an adaptive path to maximize SNR of the target return. The point at which the AUV trajectory significantly deviates from the preprogrammed path in the figure indicates when a target of interest has been declared. The color map in the figure shows the SNR of the target signal summed over the adaptive part of the AUV trajectory. Given the side-looking geometry of the sonar in this example, the adaptive behavior rule is given by

$$\hat{h}_{p+1} = \begin{cases} h_p - 5^\circ, & \Gamma_p(x_t, y_t) \geq \Gamma_{p-1}(x_t, y_t) \\ h_p + 5^\circ, & \text{otherwise} \end{cases} \quad (17)$$

where h_p is the desired heading at the time of ping p . This particular adaptive behavior rule is somewhat simplistic, but it takes advantage of the monostatic sonar geometry by turning toward the side-looking source as the detection statistic increases. In effect, the vehicle tries to maintain the target of interest in the main lobe of the source while moving forward. The result is that the vehicle circles the target, as can be seen in the figure. During the circuit around the target, target classification methods such as those described in this paper are applied to further reduce the false alarm rate for mine detection. Upon completion of the circuit, the vehicle is positioned and ready to continue its preprogrammed mission.

D. Classification Examples

Examples of mine classification through PSD and bispectrum analysis are shown in this section using real data collected from the GOATS 1998 [1] and GOATS 2002 experiments, as well as simulated data generated using SEALAB. Although the exact

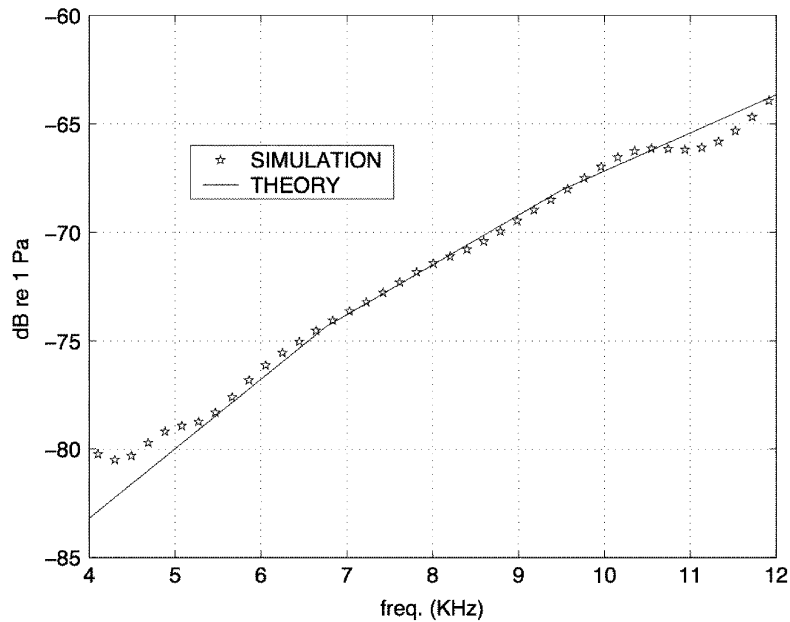


Fig. 7. Theoretical and simulated reverberation PSD.

experimental conditions cannot be perfectly known, the experimental scenario is reproduced in each case with the highest fidelity possible.

In the first subsection, the acoustic simulation tool is used and its strengths and weaknesses briefly discussed. The following two subsections show the numerical results for the GOATS 1998 and GOATS 2002 experimental scenario, respectively. In both cases, the SEALAB simulation tool is run as a theoretical baseline for comparison. In all the examples the targets are 1 m diameter buried spheres, with the center of the sphere positioned at 0.5 m under the bottom surface. The classification is achieved by applying the full CDAC processing on the simulated or experimental time series just as it would be implemented onboard the AUV. The detection algorithm proposed in Section II is first applied to the data to detect the presence and the position of the targets. Once a detection has occurred, the classification algorithm is applied to the data inside the elastic search window. The PSD and the bispectrum of the received signal are then compared to the reverberation-only PSD and bispectrum, respectively. In the numerical examples the filtering windows in (12) and (13) are chosen to be the Hamming window.

1) *SEALAB Acoustic Simulated Data*: Before using the simulation tool to recreate the experimental scenario, the PSD calculated from simulated data is compared with the PSD derived from a theoretical model which considers only surface scattering [16]. The reverberation second-order statistics are derived for a linear geometry, assuming that the water column and the lower bottom are homogeneous media with constant density and sound speed. A constant density, but random sound speed profile medium is positioned between the two homogeneous media. The density and the sound speed mean value are equal to those of the homogeneous lower medium. The parameter values used in the examples are reported in Table I. Fig. 6 shows the reverberation PSD and corresponding autocorrelation function (ACF) computed for a planar wave impinging on the

sea bottom as described above. A slightly more realistic model, which involves cylindrical geometry consideration, is considered in [17]. However, the most significant omission of the simulations is expected to be that of sub-bottom volume scattering. This phenomenon indeed appears clearly in the following numerical examples, as will be discussed in the following section.

The PSD shown in Fig. 6 is integrated at each frequency over the wave number plane to simulate the source beam, and it is then possible to compare it with the PSD calculated from the time series generated by SEALAB. The result in Fig. 7 shows a very good agreement between theoretical and simulated results. The PSD are evaluated in dB re 1 Pa. Having established the consistency between analytical results and the reverberation signals generated by SEALAB, the SEALAB-generated results will be used as the theoretical baseline for comparison with GOATS experimental data in the following examples.

2) *GOATS 1998 Experimental Data*: The plots in Fig. 8 show the estimated PSD when the sphere is present in the target field as well as the reverberation-only estimated PSD for the experimental and simulated data, respectively. The data used to estimate the reverberation PSD are collected inside the same temporal window that was established after the specular detection has occurred, in order to process data backscattered from the same spatial field. The reverberation data are collected before the detection, when no target is present in the illuminated patch. Fig. 8 shows the experimental results, as well as the simulation results, and the estimated PSD when the target is simulated as a rock. The PSDs are evaluated in dB re 1 Pa and the frequency axis is in kHz. Both experimental and simulated data show that the elastic response is a valuable means to discriminate man-made objects, such as mines, against natural objects, such as rocks. The natural frequency-selectivity of the elastic targets causes the peaks of the elastic response to show up at specific frequencies, thus making the use of spectral analysis a powerful means to discriminate such peaks. The

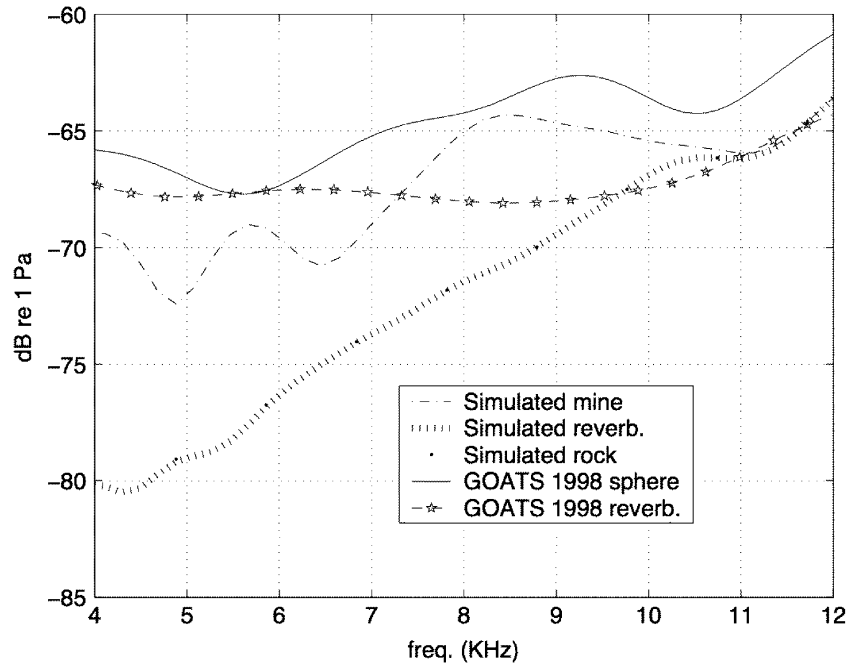


Fig. 8. Sphere PSD estimation compared to the reverberation and rock spectra, using the GOATS 1998 and simulated data.

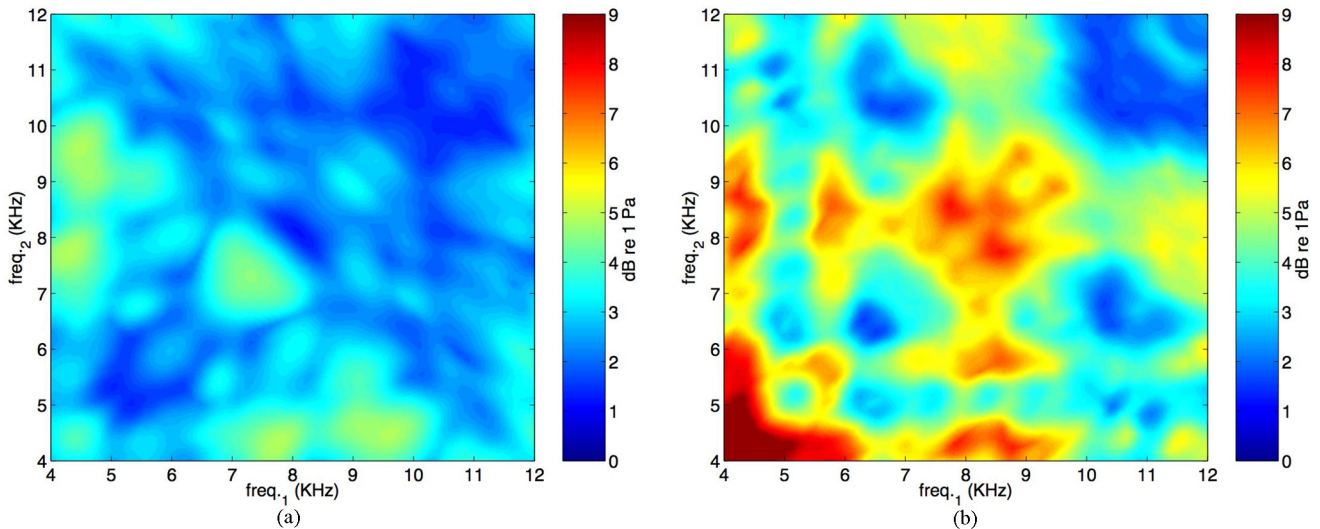


Fig. 9. Sphere bispectrum gain over reverberation, using the GOATS 1998 and simulated data. (a) Experimental data. (b) Simulated data. (Color version available online at <http://ieeexplore.ieee.org>.)

peaks stand up to 5 dB over the reverberation for experimental data and the total gain computed as in (14) is $\gamma_2 = 3.0535$ dB. As previously documented, the simulation tool neglects the sub-bottom volumetric scattering that becomes significant at lower frequencies. This omission is evident in Fig. 8 and is believed to be partly responsible for the apparent higher gain achieved in simulation ($\gamma_2 = 6.0869$ dB). Finally, it is worthwhile to note that when the target sphere is a rigid rock there is no elastic response following the specular response and the PSD is the same as the PSD of the reverberation signal ($\gamma_2 = 0$ dB), as shown in Fig. 8

Fig. 9 shows the modulus of the elastic sphere-plus-reverberation bispectrum normalized to the modulus of the reverberation bispectrum, using the same experimental and simulated data as in the previous example. The normalized bispectra are shown

in dB re 1 Pa, and the frequency units in the axis are kHz, as in the previous example. The results obtained by applying the third-order spectral analysis show the presence of a significant gain in the experimental data when the target is a mine-like object, with peaks over 5 dB with respect to the reverberation. The total gain, computed as in (15), is $\gamma_3 = 4.3066$ dB for the experimental data, and $\gamma_3 = 7.5486$ dB for the simulated data. The same quantities calculated for a simulated rock-like target give rise to a unit gain (i.e., $\gamma_3 = 0$ dB), due to the fact that the signal received inside the elastic window has the same statistical properties as the reverberation, causing the normalized bispectrum to equal 0 dB over the entire frequency plane.

These examples confirmed that the computation of the bispectrum allows a higher gain than the PSD, i.e., $\gamma_3 > \gamma_2$ for both experimental and simulated data.

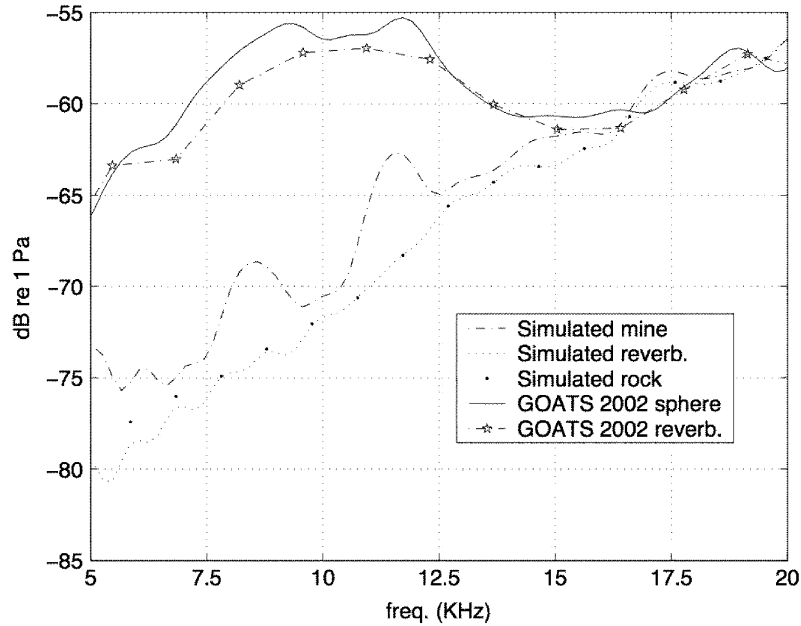


Fig. 10. Sphere PSD estimation compared to the reverberation and rock spectra, using the GOATS 2002 and simulated data.

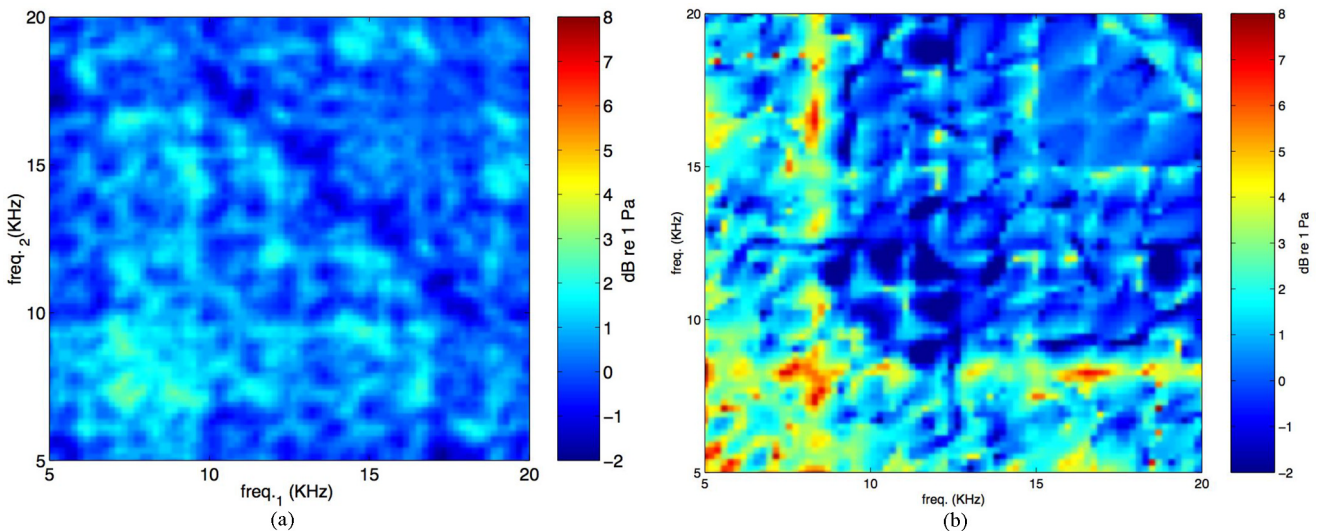


Fig. 11. Sphere bispectrum gain over reverberation, using the GOATS 2002 and simulated data. (a) Experimental data. (b) Simulated data. (Color version available online at <http://ieeexplore.ieee.org>.)

3) *GOATS 2002 Experimental Data*: The same quantities calculated in the previous subsection are now computed using the GOATS 2002 experimental data. Fig. 10 shows the estimated PSD of the sphere-plus-reverberation signal compared to the estimated reverberation PSD for both experimental and simulated data. As in the previous example, the estimated PSD for the simulated data is also plotted when the target sphere is modeled as a rock. For both the experimental and simulated data, the elastic peaks are clearly distinguishable from the reverberation spectrum, although these peaks appear to be more pronounced in the simulated data. As previously discussed for the GOATS 1998 data, the PSD for the rock target is the same as the reverberation PSD, because the target does not radiate elastic waves into the ocean. For the experimental data, the elastic response shows peaks up to 2 dB with respect to the reverberation, and the total gain is $\gamma_2 = 1.0673$ dB. Again, it can be inferred from the experimental data that the bottom scattering process is dom-

inant over the surface scattering at the lower frequencies. The volume scattering dominance in this case goes up to 15 kHz as opposed to 10 kHz in the previous example. This increased frequency range is probably due to the higher grazing angle in the GOATS 2002 experiment (25 degrees versus 16.2 degrees), which leads to increased sub-bottom penetration. The resulting increase in volume scattering follows intuitively, although more rigorous proof of this effect has been demonstrated both theoretically and experimentally [18]. In the simulated case, the total gain is $\gamma_2 = 1.9156$ dB.

Fig. 11 shows the modulus of the mine-like target-plus-reverberation bispectrum normalized to the modulus of the corresponding reverberation bispectrum, for both experimental and simulated data. In both cases it is possible to classify the mine-like object, because the target bispectrum gains up to 3.5 dB for the experiment and up to 7.5 dB for the simulation. The higher gain at the lower frequencies for the simulated data is in agree-

ment with the plots in Fig. 10. The total gains are $\gamma_3 = 1.1770$ dB and $\gamma_3 = 3.1509$ dB for the experimental and simulated data, respectively.

In conclusion, as in the previous example, the bispectrum of fers improved classification capabilities compared to the PSD, and the improvement is higher for the simulated data. The gains γ_2 and γ_3 obtained for the GOATS 2002 experiment are lower than the corresponding gains obtained for the GOATS 1998 experiment, due the higher reverberation levels in the GOATS 2002 scenario caused by the wide-beam source. The generally higher gains achieved in the simulation are again a result of the fact that the simulation tool neglects the volume scattering process.

V. CONCLUSION

A two-stage system for CDAC of mine-like objects has been presented and shown to be effective in theory, simulation and live experiments. The HOS classification method shows a significant improvement over classical spectral estimation in simulation. In at-sea experiments the classification advantage of the higher order method is diminished, likely due to the less Gaussian statistics of the sub-bottom volume inhomogeneities. These results, although they are from two very different live at-sea experiments with AUVs, illustrate a common feature of automatically detectable elastic returns using the proposed CDAC algorithm. Further enhancement of the classification is achievable through the use of adaptive vehicle motions, but this approach has yet to be successfully used in practice. While the experiments were chosen to closely resemble realistic mine-hunting situations, they are limited due to the use of canonical mine-like targets and a relatively clutter-free environment. It remains to be seen whether the elastic returns of real mines will be detectable for this classification process, as well as whether the HOS classification advantage will be maintained. This will be the target of future experiments and analysis.

ACKNOWLEDGMENT

The authors would like to thank all of the scientists, engineers, technicians, and program managers who have made the GOATS project such a success. They would like to especially thank M. Mazzi, P. Guerrini, and E. Bovio of NATO SACLANTCEN, R. Damus, S. Desset, and J. Morash of the MIT AUV Laboratory, P. Newman of Oxford University (formerly of MIT), and the ONR program managers J. Simmen, T. Swean, R. Jacobson, and B. Johnson.

REFERENCES

- [1] J. Edwards, H. Schmidt, and K. LePage, "Bistatic synthetic aperture target detection and imaging with an AUV," *IEEE J. Ocean. Eng.*, vol. 26, no. 4, pp. 690–699, Oct. 2001.
- [2] Y. Zhang, A. Baggeroer, and J. Bellingham, "Spectral-feature classification of oceanographic processes using an autonomous underwater vehicle," *IEEE J. Ocean. Eng.*, vol. 26, no. 4, pp. 726–741, Oct. 2001.
- [3] J. Edwards and H. Schmidt, "Real-time classification of buried targets with teams of unmanned vehicles," in *Proc. Marine Technology Society (MTS)/IEEE OCEANS 2002: Reflections of the Past, Visions of the Future*, Biloxi, MS, 2002, pp. 316–319.

- [4] A. Oppenheim and R. Schaffer, *Discrete-Time Signal Processing*. Englewoods Cliffs, NJ: Prentice Hall, 1999.
- [5] A. Pezeshki, M. Azimi-Sadjadi, L. Scharf, and M. Robinson, "Underwater target classification using canonical correlations," in *Proc. IEEE Oceans 2003 Conf.*, vol. 4, Sep. 2003, pp. 1906–1911.
- [6] S. Ji, X. Liao, and L. Carin, "Adaptive multi-aspect target classification and detection with hidden markov models," in *Proc. Int. Conf. Acoustics, Speech and Signal Processing*, vol. 2, May 2004, pp. 125–128.
- [7] J. Malas, K. Pesala, and J. Westercamp, "Automatic target classification of slow moving ground targets in clutter," *IEEE Trans. Aerosp. Electron. Syst.*, vol. 40, no. 1, Jan. 2004.
- [8] M. Pinto, A. Bellettini, R. Hollett, and A. Tesei, "Real- and synthetic-array signal processing of buried targets," *IEEE J. Ocean. Eng.*, vol. 27, no. 3, pp. 484–494, Jul. 2002.
- [9] C. L. Nikias and A. P. Petropulu, *Higher-Order Spectra Analysis*. Englewoods Cliffs, NJ: Prentice Hall, 1993. ser. Signal Processing Series.
- [10] Y. Doisy, "General motion estimation from correlation sonar," *IEEE J. Ocean. Eng.*, vol. 23, no. 2, pp. 127–140, Apr. 1998.
- [11] P. Stoica and R. Moses, *Introduction to Spectral Analysis*. Englewoods Cliffs, NJ: Prentice Hall, 1997.
- [12] H. Schmidt, "Numerically stable global matrix approach to radiation and scattering from spherically stratified shells," *J. Acoust. Soc. Am.*, vol. 94, no. 4, 1993.
- [13] *This is the Moos*, P. Newman. (2001). [Online]. Available: <http://oceanai.mit.edu/pnewman/MOOS>
- [14] W. W. Au, *The Sonar of Dolphins*. New York: Springer-Verlag, 1993.
- [15] *U.S. Navy Enlists the Help of Marine Mammals to Secure Iraqi Ports*, K. Schmidt. (2003). [Online]. Available: <http://usinfo.state.gov/regional/nea/iraq/text2003/0418navy.htm>
- [16] F. Bass and I. Fuks, *Wave Scattering from Statistically Rough Surfaces*. Oxford: Pergamon, 1979.
- [17] K. D. LePage and H. Schmidt, "Spectral integral representations of monostatic back scattering from three-dimensional distributions of sediment volume inhomogeneities," *J. Acoust. Soc. Am.*, vol. 113, no. 1, Jan. 2003.
- [18] D. R. Jackson and K. B. Briggs, "High-frequency bottom backscattering: Roughness versus sediment volume scattering," *J. Acoust. Soc. Am.*, vol. 92, no. 2, pp. 962–977, Aug. 1992.



Monica Montanari received the Laurea degree (*cum laude*) and the Ph.D. degree in telecommunications engineering from the University of Pisa, Pisa, Italy, in 1998 and 2002, respectively.

From February to August 2000, she was a Research Assistant at the NATO SACLANT Undersea Research Centre, La Spezia, Italy. In 2002, she joined the former Department of Ocean Engineering at the Massachusetts Institute of Technology, Cambridge, as a Postdoctoral Associate. In 2005, she joined VASA Associates, McLean, VA, as a Senior Scientist. Her general research interests are in the areas of statistical signal and array processing, detection, estimation, and classification, with application to radar and sonar processing.



Joseph R. Edwards received the B.S.M.E. and M.S.M.E. degrees from Virginia Polytechnic Institute and State University, Blacksburg, in 1994 and 1996, respectively, and the Ph.D. degree in ocean engineering from Massachusetts Institute of Technology (MIT), Cambridge, in 2006.

In 1996–1999, he was an Acoustic Engineer for the Engineering Technology Center, Mystic, CT. He was a Summer Research Assistant at the NATO SACLANT Undersea Research Centre, in 2000. His research interests are in signal and information processing and acoustics, particularly as applied to multiplatform detection and classification of buried targets.



Henrik Schmidt received the M.S. and Ph.D. degrees in civil engineering from The Technical University of Denmark, Lyngby, Denmark, in 1974 and 1978, respectively.

From 1978 to 1982, he worked as a Research Fellow at Risoe National Laboratory in Denmark. From 1982 to 1987, he worked as Scientist and Senior Scientist at the NATO SACLANT ASW Research Centre, Italy. He has been on faculty of the Massachusetts Institute of Technology (MIT), Cambridge, since 1987. He has served as Associate

Director of Research at the MIT Sea Grant College Program, from 1989 to 2002, and as the Associate Department Head, in 1994–2002. He served as the Acting Department Head of Ocean Engineering, from 2002 to 2004. Currently, he is Professor of Mechanical and Ocean Engineering at MIT. He has been Principal Investigator in two Arctic ice station experiments, and Chief Scientist for several recent, major experiments in coastal environments. He has developed numerically efficient numerical algorithms for propagation of acoustic and seismic waves in the ocean and solid earth environment, including the SAFARI code and its successor OASES which is used as a reference propagation model in more than 100 institutions around the world, including all US Navy laboratories and most major universities involved in underwater acoustics and seismic research. The OASES code is also used extensively by several private DoD contractors as part of their sonar processing, and by the oil exploration community. In recent years, he has been pioneering the development of new underwater acoustic sensing concepts for networks of small autonomous underwater vehicles (AUV). Thus, in collaboration with SACLANT Undersea Research Centre he is exploring the possibility of using AUVs for measuring the three-dimensional acoustic scattering from the seabed to detect and identify buried objects, with application to mine countermeasures and environmental management in the littoral ocean. In addition, he has been leading the development of a synergy of ocean acoustic tomography and direct sampling by autonomous underwater vehicles for observation and forecasting of ocean processes on multiple scales. He has authored many articles on underwater acoustics, seismics, and signal processing, and has coauthored a textbook on computational ocean acoustics. His research has focused on underwater acoustic propagation and signal processing, in particular on the interaction of sound in the ocean with seismic waves in the ocean bottom and the Arctic ice cover. His work has been of theoretical, numerical, and experimental nature.

Prof. Schmidt is a Fellow of the Acoustical Society of America (ASA). He served as Chairman of the ASA Technical Committee on Underwater Acoustics, from 1991 to 1994 and he is currently an Elected Member of the Executive Council of ASA. He is the 2005 Recipient of the ASA Pioneer of Underwater Acoustics medal.